Light-trapping in perovskite solar cells

Qing Guo Du, Guansheng Shen, and Sajeev John

Articles you may be interested in

Light-trapping optimization in wet-etched silicon photonic crystal solar cells
J. Appl. Phys. **118**, 023103 (2015); 10.1063/1.4926548

Effect of textured electrodes with light-trapping on performance of polymer solar cells
J. Appl. Phys. **111**, 104516 (2012); 10.1063/1.4720083

Integrated photonic structures for light trapping in thin-film Si solar cells
Appl. Phys. Lett. **100**, 111110 (2012); 10.1063/1.3693613

Efficient polymer solar cells based on light-trapping transparent electrodes
Appl. Phys. Lett. **100**, 103303 (2012); 10.1063/1.3691906

Photonic crystal enhanced light-trapping in thin film solar cells
J. Appl. Phys. **103**, 093102 (2008); 10.1063/1.2908212

Light-trapping in perovskite solar cells

Qing Guo Du,[1,2,a] Guansheng Shen,[1,3] and Sajeev John[1,4]

[1]*Department of Physics, University of Toronto, 60 ST. George St., Toronto, Ontario, M5S 1A7, Canada*
[2]*Institute of High Performance Computing, A* STAR, Singapore, 138632, Singapore*
[3]*School of Information and Communication Engineering, Beijing University of Posts and Telecommunications, Beijing 100876, China*
[4]*Department of Physics, Soochow University, Suzhou, China*

We numerically demonstrate enhanced light harvesting efficiency in both $CH_3NH_3PbI_3$ and $CH(NH_2)_2PbI_3$-based perovskite solar cells using inverted vertical-cone photonic-crystal nanostructures. For $CH_3NH_3PbI_3$ perovskite solar cells, the maximum achievable photocurrent density (MAPD) reaches 25.1 mA/cm^2, corresponding to 92% of the total available photocurrent in the absorption range of 300 nm to 800 nm. Our cell shows 6% absorption enhancement compared to the Lambertian limit (23.7 mA/cm^2) and has a projected power conversion efficiency of 12.9%. Excellent solar absorption is numerically demonstrated over a broad angular range from 0 to 60 degree for both S- and P- polarizations. For the corresponding $CH(NH_2)_2PbI_3$ based perovskite solar cell, with absorption range of 300 nm to 850 nm, we find a MAPD of 29.1 mA/cm^2, corresponding to 95.4% of the total available photocurrent. The projected power conversion efficiency of the $CH(NH_2)_2PbI_3$ based photonic crystal solar cell is 23.4%, well above the current world record efficiency of 20.1%. © 2016 Author(s). All article content, except where otherwise noted, is licensed under a Creative Commons Attribution (CC BY) license (*http://creativecommons.org/licenses/by/4.0/*). [http://dx.doi.org/10.1063/1.4953336]

I. INTRODUCTION

Metal halide perovskites have been intensively studied in solar cell applications since the first perovskite solar cell was reported.[1] The excellent optical and electrical properties of perovskites make them among the most promising next generation solar cells. Both mesostructured and planar perovskite architectures have been proposed and their power conversion efficiency (PCE) has improved very rapidly in recent years.[2–12] There are currently two distinct perovskite family materials, $CH_3NH_3PbI_3$ and $CH(NH_2)_2PbI_3$, used in solar cell research. The absorption spectrum of $CH_3NH_3PbI_3$ is from 300 nm to 800 nm while $CH(NH_2)_2PbI_3$ has a broader spectrum from 300 nm to 850 nm. Consequently, $CH(NH_2)_2PbI_3$ enables higher power conversion efficiency than $CH_3NH_3PbI_3$ based solar cells. Most recently, a 20.1% PCE solar cell has been certified in a $CH(NH_2)_2PbI_3$ planar device architecture.[13] While previous attention has been focused on improving electronic quality of the perovskite layer, there remain opportunities to optimize optical absorption through light-trapping. For planar perovskite solar cells, the optical properties have been well studied[14] and attempts to improve the solar absorption in the perovskite active layer have focused on tandem solar cell structures.[15,16] Light-trapping has proved beneficial in Silicon, Gallium Arsenide and organic solar cells.[17–22] Light absorption enhancement and PCE improvement have been demonstrated both experimentally and theoretically. However, light-trapping enhancements have not yet been fully exploited in perovskite solar cells.

---

[a]Author to whom correspondence should be addressed, electronic mail: duqi0001@e.ntu.edu.sg.

In this paper, we numerically simulate solar absorption in nanostructured perovskite solar cells. By direct solution of Maxwell's equations, we identify optimized light-trapping architectures consisting of inverted-vertical-cone arrays. The active layer thickness is limited to about 300 nm of perovskite material to ensure charge carrier collection. This corresponds to an "equivalent bulk thickness" of 180 nm. Absorption and reflection are calculated using the finite-difference time-domain (FDTD) method for the absorption wavelength ranges of both perovskites using a 5 nm step size.[23] The lattice constant of the photonic crystal and the base radius of the inverted cone are optimized to provide the best absorption, expressed as a maximum achievable photocurrent density (MAPD).

For $CH_3NH_3PbI_3$ perovskite, the total available photocurrent from sunlight from 300 nm to 800 nm is 27.2 mA/cm^2. We identify an inverted-vertical-cone photonic crystal with MAPD of 25.1 mA/cm^2. This is 92% of the total available photocurrent and exceeds the Lambertian limit (23.7 mA/cm^2)[19] for an equivalent thickness of 180 nm. For the $CH(NH_2)_2PbI_3$ perovskite, the total available photocurrent from sunlight from 300 nm to 850 nm is 30.5 mA/cm^2. In this case, we identify a photonic crystal architecture that yields 29.1 mA/cm^2, corresponding to 95.4% of the total available sunlight.

II. ELECTROMAGNETIC SIMULATION

A single unit cell of our perovskite photonic crystal solar cell is shown in Fig. 1. From bottom to top, the device consists of (i) perfect electronic conductor (PEC) lower contact, (ii) PCBM hole blocker, (iii) perovskite active region ($CH_3NH_3PbI_3$ or $CH(NH_2)_2PbI_3$) and (iv) PEDOT electron blocker. The ITO top contact is a 60 nm thick conformal coating on the PEDOT layer and the remainder of the conical pore is filled with glass (SiO_2) for encapsulation. The lattice constant, a, of the periodic structure and the cone base radius, R, are parameters that are optimized for maximum solar absorption. For simplicity, we neglect the imaginary parts (k) of the refractive indices of PEDOT, PCBM and ITO. The real parts of the refractive indices of PEDOT and PCBM are chosen as 1.6 and 2.1 respectively.[11] The real part of the refractive index of ITO is chosen as 1.5,[24] the same as glass. These numbers are approximate, but illustrate the solar absorption enhancement in perovskite photonic crystals due to light-trapping.

A full three-dimensional FDTD method is employed for all numerical calculations. Periodic boundary conditions are used in the x-, y-directions and perfectly matched layers (PMLs) are used in the z-direction. The simulation region in the x- and y-directions is chosen to be one unit cell. Light is incident on the cell from the top of the structure in Fig. 1. During the numerical simulation,

(a)   (b)
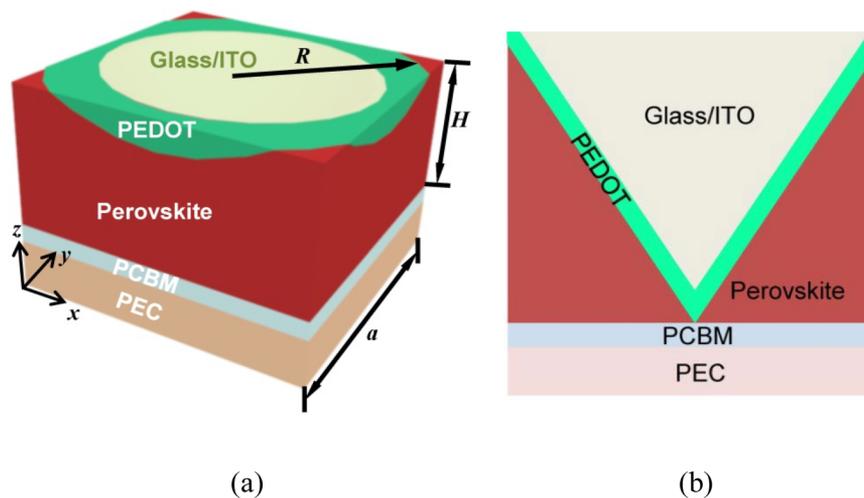
FIG. 1. (a) Three-dimensional perspective of the inverted vertical cone perovskite unit cell, (b) Two-dimensional side view of the device unit cell.

the amplitudes of the reflected and transmitted waves are recorded, transformed to the frequency domain and normalized by the incident spectrum. In this way, we obtain the transmission $T(\omega)$ and reflection $R(\omega)$ coefficients. The absorption coefficient $A(\omega)$ is then determined by

$$A(\omega) = 1 - R(\omega) - T(\omega) \tag{1}$$

Knowing the fraction of incident light absorbed by the active layer and assuming all generated carriers are collected, the MAPD is given by:

$$J_{MAPD} = \int_{300\ nm}^{\lambda_{max}} \frac{e\lambda}{hc} I(\lambda)A(\lambda)d\lambda \tag{2}$$

Here, e is the electron charge, λ is the vacuum wavelength, h is Plank's constant and c is the speed of light in vacuum. For $CH_3NH_3PbI_3$, $\lambda_{max} = 800$ nm, whereas, for $CH(NH_2)_2PbI_3$, $\lambda_{max} = 850$ nm. $I(\lambda)$ is the solar intensity of the Air Mass 1.5 (*AM* 1.5) solar spectrum,[25] and $A(\lambda)$ is the absorption coefficient in the active layer obtained from Eqn. (1).

III. CH$_3$NH$_3$PbI$_3$ BASED SOLAR CELLS

The refractive index of $CH_3NH_3PbI_3$[26] is shown in Fig. 2. In our numerical simulation of sunlight absorption, the thicknesses of PCBM and PEDOT are both fixed at 10 nm. The total height of the active perovskite region is fixed at $H = 300$ nm (see Fig. 1(a)) to ensure reasonable carrier collection efficiency.[27] The optimization process is performed by varying the lattice constant a from 200 nm to 1000 nm and the base radius R of the inverted cone from $a/4$ to $3a/4$. The MAPD map is shown in Fig. 3. When $a = 600$ nm and $R = 380$ nm, the maximum MAPD of 24.0 mA/cm^2 is realized. The total equivalent bulk thickness of perovskite material in this case is 180 nm of a corresponding planar device.

The absorption and reflection spectra of the optimized device structure are shown in Fig. 4. The spectrum of a corresponding planar device is also shown for reference. For the planar reference cell, the thickness of PCBM and PEDOT are both fix at 10 nm. The thickness of ITO is likewise 60 nm. Clearly, absorption in the optimized photonic crystal is better than the planar one throughout wavelength range from 300 nm to 800 nm. We observe a large absorption enhancement in the wavelength range from 750 nm to 800 nm with an absorption peak at 781 nm, where the absorption is very low for the planar device.

Fig. 5 shows the field intensity distribution and the Poynting vector at 781 nm (absorption peak in Fig. 4) in the *x*-*z* plane bisecting the cone. The high field intensity spot near the bottom of the conical pore has a peak enhancement of 50 as indicated by the color bar. This localized resonance mode extends into the nearby perovskite with intensity enhancement in the range of 10-15. The
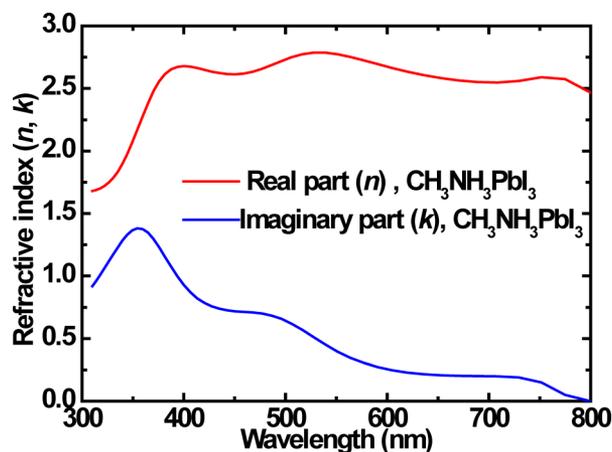
FIG. 2. Refractive index (real part n and imaginary part k) of CH$_3$NH$_3$PbI$_3$ as reported in Ref. 26.
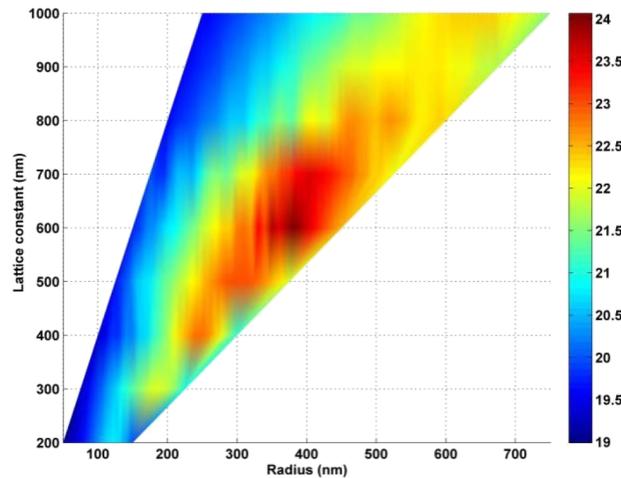
FIG. 3. MAPD optimization map for $CH_3NH_3PbI_3$ based perovskite photonic crystal with lattice constant a from 200 nm to 1000 nm and cone base radius R from $a/4$ to $3a/4$.

Poynting vector exhibits a circulation pattern around the localized hot spot, consistent with a long optical dwell time and strong absorption in the perovskite film.

In order to further reduce the reflection from the top surface, a glass dome is placed on top of each unit cell as shown in the insert of Fig. 6 (2D side view of the device structure). The base radius of the glass dome is fixed at 380 nm (the same as the base radius of the inverted vertical cone) and antireflection behavior is optimized by varying the height (indicated as h in the insert of fig. 6) of the dome from 100 nm to 500 nm. The optimized height of the glass dome is $h = 300$ nm. The absorption spectra of the optimized inverted cone device with and without the dome are shown in Fig. 6. With this anti-reflection coating, the absorption is enhanced for wavelengths longer than 500 nm, leading to an improved MAPD of 24.3 mA/cm^2. For an equivalent bulk thickness of $L = 180$ nm of $CH_3NH_3PbI_3$, the absorption spectrum in the "Lambertian limit"[19,28] is given by:

$$A = 1 - \frac{1}{1 + \alpha 4 n^2 L} \tag{3}$$
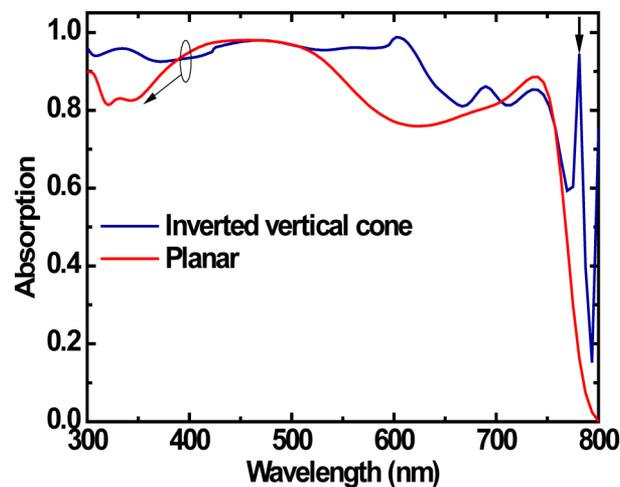
FIG. 4. Simulated absorption and reflection spectra of the optimized ($a = 600$ nm, $R = 380$ nm) inverted cone photonic crystal and planar $CH_3NH_3PbI_3$ solar cells. The $CH_3NH_3PbI_3$ thickness of the planar cell is 180 nm, corresponding to the "equivalent bulk thickness" of $CH_3NH_3PbI_3$ in the inverted-cone photonic-crystal device.
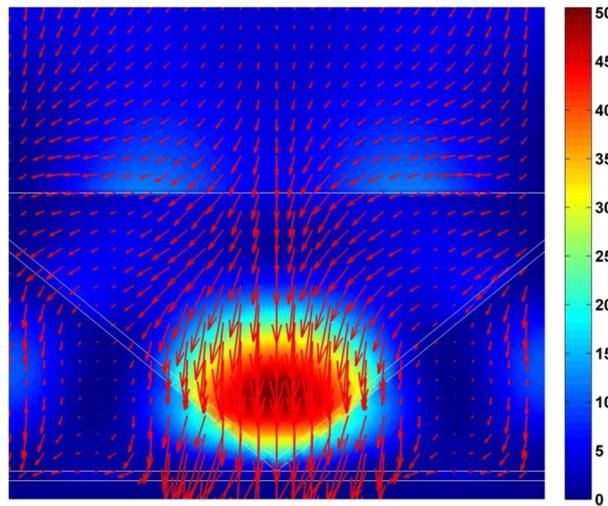
FIG. 5. Field intensity distribution and Poynting vector-field map at 781 nm in the CH$_3$NH$_3$PbI$_3$-based inverted cone device with a = 600 nm and R = 380 nm.

Here $\alpha = 4\pi k \lambda$ is the absorption coefficient, n and k are the real and imaginary parts of the refractive index of CH$_3$NH$_3$PbI$_3$. The Lambertian absorption benchmark is shown in Fig. 6, as a dashed black line and yields the MAPD of 23.7 mA/cm^2.

The ability to absorb sunlight at off-normal incidence over a wide angular range for both polarizations is important for solar cell designs without an expensive solar tracking system. In Fig. 7, we present numerical results on the dependence of MAPD on incident angle for our optimized CH$_3$NH$_3$PbI$_3$ perovskite, inverted cone, solar cell (with glass dome on top) for both *S*- (no electric field in *z* direction) and *P*- (no magnetic field in z direction) polarizations. The MAPD dependence on incident angles of both S- and P- polarizations for the planar cell are listed as a reference. For both polarizations, the MAPD of our optimized, inverted cone, solar cell has no substantial degradation for incident angles up to 60 degrees. This is in contrast to the planar perovskite solar cell where both S- and P- polarizations show lower and gradually decreasing MAPD for incident angles from 5 to 70 degrees.

Finally, we consider the insertion of a thin layer of bulk CH$_3$NH$_3$PbI$_3$ between the inverted cone layer and the bottom PCBM layer. The thickness, l, of the extra bulk CH$_3$NH$_3$PbI$_3$ is optimized in
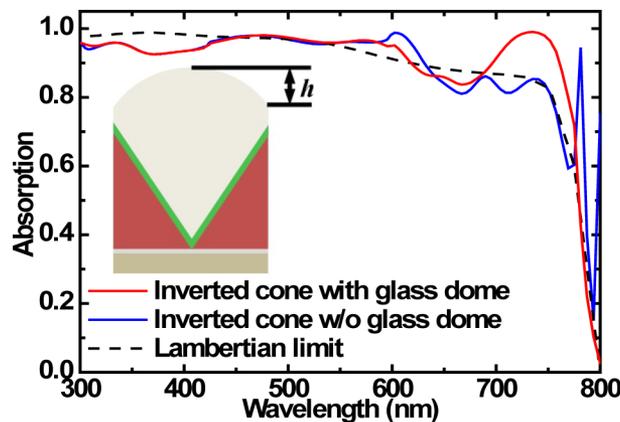
FIG. 6. Simulated absorption spectra of the optimized CH$_3$NH$_3$PbI$_3$ based inverted cone perovskite solar cell with (red curve) and without (blue curve) antireflection glass dome (h = 300 nm) compared with the "Lambertian limit" (dashed line), for an equivalent bulk CH$_3$NH$_3$PbI$_3$ thickness of 180 nm.
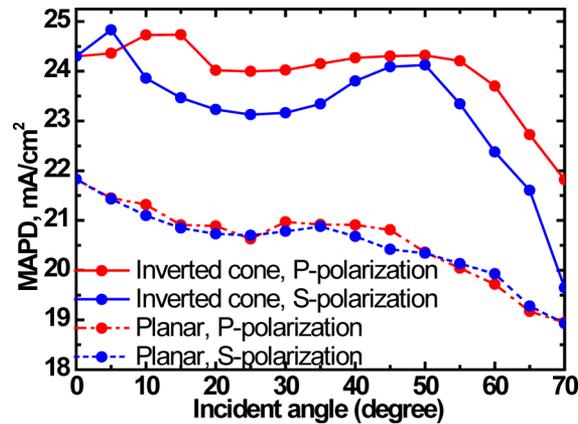
FIG. 7. MAPD at oblique incidence from 5 to 70 degrees for both s and p polarizations for our optimized $CH_3NH_3PbI_3$ conical pore photonic crystal (with a glass dome anti-reflection) with $a = 600$ nm, $R = 380$ nm and dome height $h = 300$ nm. Also shown (dashed curves) are MAPD at oblique incidence from 5 to 70 degrees for both s and p polarizations for the planar counterpart with 180 nm equivalent bulk thickness of $CH_3NH_3PbI_3$.

the range from 20 nm to 100 nm as shown in Table. I. The optimum thickness of bulk $CH_3NH_3PbI_3$ is 40 nm, providing a MAPD of 25.1 mA/cm^2, corresponding to absorption of 92% of sunlight.

The PCE of a real-world planar cell with a 180 nm $CH_3NH_3PbI_3$ perovskite is 11.2%.[11] We obtain a projected efficiency for our photonic crystal solar cell by assuming the same open circuit voltage and fill factor as in the planar cell. Our numerical simulation yields a MAPD of the planar cell of 21.8 mA/cm^2 compared to 25.1 mA/cm^2 for the optimized device structure with $a = 600$ nm, $R = 380$ nm, $h = 300$ nm and $l = 40$ nm. Accordingly, we project an efficiency of 12.9% for our $CH_3NH_3PbI_3$ based, perovskite photonic crystal solar cell.

IV. CH(NH$_2$)$_2$PbI$_3$ BASED SOLAR CELLS

Given the broader (300 nm – 850 nm) absorption spectrum of $CH(NH_2)_2PbI_3$, a higher MAPD and PCE are realized for this type of perovskite. Since, the refractive index of $CH(NH_2)_2PbI_3$, to the best of our knowledge, is not fully tabulated in the wavelength range from 300 nm to 850 nm, we infer it from the following considerations. The imaginary part of the refractive index of $CH(NH_2)_2PbI_3$ from 500 nm to 850 nm is tabulated.[29] However, the absorption spectra for both $CH(NH_2)_2PbI_3$ and $CH_3NH_3PbI_3$ are nearly the same in wavelength from 300 nm to 500 nm.[30] Accordingly, we adopt the imaginary part of the refractive index of $CH_3NH_3PbI_3$ to represent that of $CH(NH_2)_2PbI_3$ in wavelength from 300 nm to 500 nm. Small differences in the real part of the refractive index have little influence on the absorption. Accordingly, we adopt the real part of the refractive index of $CH_3NH_3PbI_3$ in wavelength from 300 nm to 800 nm and stretch it linearly from 300 nm to 850 nm. We use this stretched real part of the refractive index to represent that of $CH(NH_2)_2PbI_3$. The inferred real and imaginary parts of the refractive index of $CH(NH_2)_2PbI_3$

TABLE I. MAPD of optimized device with an extra thickness (l) of bulk $CH_3NH_3PbI_3$ layer inserted between inverted cone layer and PCBM layer.

Bulk $CH_3NH_3PbI_3$ thickness l (nm)	MAPD (mA/cm^2)
20	24.7
40	25.1
60	24.7
80	24.5
100	24.6
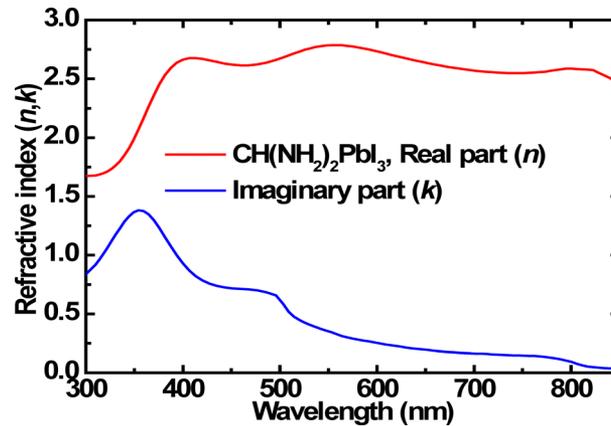
FIG. 8. Estimated Refractive index (real part, n and imaginary part, k) of $CH(NH_2)_2PbI_3$.

are shown in Fig. 8. The additional range of weak absorption from 800-850 nm leads to a different set of optimum structural parameters for the two different materials. Our light-trapping strategy is based on parallel-to-interface refraction of incident sunlight into slow-light modes within the active range.[19,20] The efficient capture of this additional sunlight requires a modified structure.

As in the case of $CH_3NH_3PbI_3$, we now optimize the MAPD of $CH(NH_2)_2PbI_3$ using our inverted cone photonic crystal architecture. As a start, the cone height is fixed at $H = 300$ nm, the lattice constant a is varied from 300 nm to 1000 nm and the cone base radius is varied from a/4 to 3a/4. The calculated MAPD map is shown in Fig. 9(a). The optimum structure with lattice constant $a = 700$ nm and radius $R = 435$ nm provides a MAPD of 26.9 mA/cm^2.

For a planar cell structure, high quality $CH(NH_2)_2PbI_3$ films with thicknesses of 500 nm can be obtained.[13] Accordingly, we consider the influence of increased cone height, H, on the MAPD. We consider $H = 300$ nm to 500 nm in steps of 50 nm. For each cone height, the lattice constant a and the base radius R are allowed to vary and the best MAPD for each cone height is shown in Fig. 10. Second peak MAPD for cone height $H = 450$ nm is provided as a reference (red dot in Fig. 10). The MAPD increases with H from 300 nm to 450 nm but reaches a maximum value of 28.3 mA/cm^2 for $H = 450$ nm, with $a = 400$ nm and $R = 230$ nm. MAPD then decreases for $H > 450$ nm. An interesting outcome of our simulation is the discovery of three competing structures (see Fig. 9(b)) for 400 nm < H < 500 nm. The optimized lattice constant $a \approx 700$ *nm* and cone base radius $R \approx 450$ *nm* remain roughly the same for cone heights of 300 nm, 350 nm and 400 nm. However when the cone height $H = 450$ nm, there is a sudden switching to a second optimum structure with $a = 400$ nm and $R = 230$ nm. When $H = 500$ nm, the optimum architecture switches to a large lattice constant $a = 900$ nm and radius $R = 595$ nm (third peak in Fig. 9(b)), but with a slightly lower MAPD. For $CH(NH_2)_2PbI_3$ based conical pore perovskite solar cells, the optimum structure with $H = 450$ nm, $a = 400$ nm and $R = 230$ nm, yields the MAPD of 28.3 mA/cm^2. We note that the MAPD of the first optimum at $a = 800$ nm and radius $R = 510$ nm (Red dot in Fig. 10) is 28.2 mA/cm^2 which is only slight lower than the MAPD of the optimum one (28.3 mA/cm^2).

A slight improvement on this photocurrent density is obtained by adding a glass-dome anti-reflection layer on top of the solar cell compared to the solar cell without a glass-dome. The cap heights are optimized for both cases of $a = 400$ nm, $R = 230$ nm and $a = 800$ nm, $R = 510$ nm for $H = 450$ nm as shown in Fig. 11. For $a = 400$ nm, $R = 230$ nm, the dome base radius is fixed at 230 nm (the same as the base radius of the vertical cone). The optimum dome height is found to be $h = 300$ nm (dome spherical radius is 238 nm). This yields the best MAPD of 29.1 mA/cm^2. For $a = 800$ nm, $R = 510$ nm, the dome base radius is fixed at 510 nm (the same as the base radius of the vertical cone). The optimum dome height is found to be $h = 420$ nm (dome spherical radius is 520 nm). The optimum MAPD is 28.8 mA/cm^2, which is only slightly lower than the best MAPD obtained here.
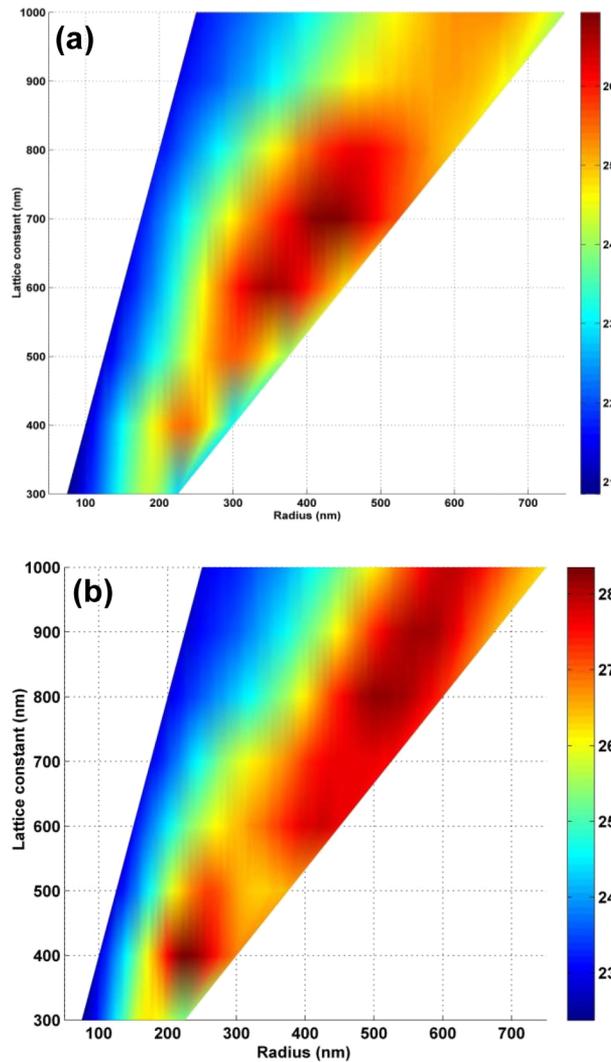
FIG. 9. MAPD optimization of CH(NH$_2$)$_2$PbI$_3$ based perovskite photonic crystal for fixed cone height (a) $H = 300$ nm, (b) $H = 450$ nm. The lattice constant a is varied from 300 nm to 1000 nm and cone base radius R is varied from $a/4$ to $3a/4$.

Finally, we consider inserting an extra bulk layer of CH(NH$_2$)$_2$PbI$_3$ between the inverted vertical cone CH(NH$_2$)$_2$PbI$_3$ layer and the PCBM layer. This strategy improved absorption in CH$_3$NH$_3$PbI$_3$, which otherwise absorbed 89% (24.3 mA/cm^2) of the total available sunlight from 300-800 nm. However, no improvement in MAPD was found by inserting a bulk layer below our optimized conical pore structure of CH(NH$_2$)$_2$PbI$_3$ with $a = 400$ nm, $R = 230$ nm and $H = 450$ nm.

Our best MAPD of 29.1 mA/cm^2 for the CH(NH$_2$)$_2$PbI$_3$ based conical pore, glass-encapsulated solar cell corresponds to absorption of 95% of all available sunlight in the 300 nm – 850 nm range. On the other hand, a world-record power-conversion efficiency of 20.1% has been reported[13] with a 500 nm planar film of CH(NH$_2$)$_2$PbI$_3$. In order to obtain a projected power-conversion efficiency for our photonic crystal design, we first calculated the MAPD of a planar CH$_3$NH$_3$PbI$_3$ device structure (glass/ITO 80 nm)/PEDOT:PSS (15 nm)/PCDTBT (5 nm)/ Perovskite (350 nm)/PC60BM (10 nm)/Ag (100 nm)) reported in Ref. 11. The short circuit in this structure is measured to be 20 mA/cm^2.[11] For this planar architecture, our calculation yields the MAPD of 21.3 mA/cm^2, using the model refractive indices obtained in Fig. 2 and assuming no absorption loss in the materials surrounding the perovskite active layer. We use this difference of 1.3 mA/cm^2 (6% of the total MAPD) as a guide to amount of additional losses not accounted by our MAPD calculation. Given
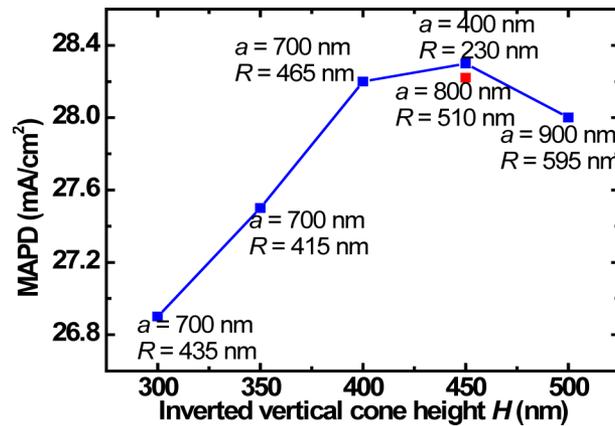
FIG. 10. Optimized MAPD versus conical pore height for $CH(NH_2)_2PbI_3$ based photonic crystal solar cell. The optimized lattice constant a and cone base radius R for each cone height are given. The second best MAPD for cone height $H = 450$ nm is provided for reference (red dot).
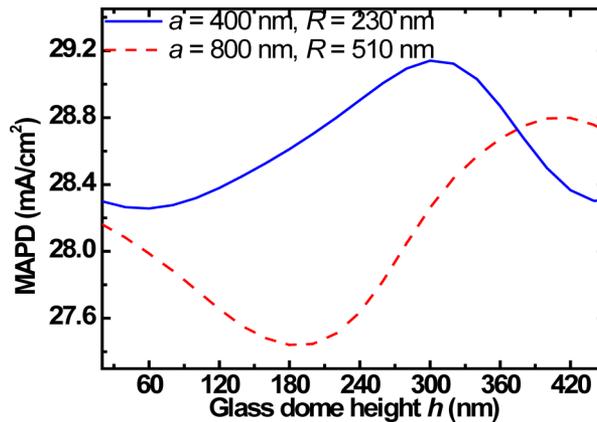
FIG. 11. MAPD versus glass dome height for optimized inverted vertical cone structure with lattice constant $a = 400$ nm, cone radius $R = 230$ nm (blue) and lattice constant $a = 800$ nm, cone radius $R = 510$ nm (red dash). For both cases, the cone height $H = 450$ nm.

the similar device structures reported in Ref. 11 and Ref. 13, we also assume the same ratio of short circuit current to MAPD (as calculated by our model) in the device[13] with reported short circuit current of 23.5 mA/cm^2 and 20.1% power conversion efficiency. Under these assumptions, the estimated MAPD of the world-record-setting $CH(NH_2)_2PbI_3$ perovskite solar cell[13] is 25.0 mA/cm^2. The projected efficiency of our $CH(NH_2)_2PbI_3$-based photonic-crystal solar cell is then estimated to be $\frac{29.1}{25} \times 20.1\% = 23.4\%$.

V. CONCLUSIONS

We have designed vertical, inverted cone, photonic-crystal light-trapping architectures for the two different perovskite solar cells involving either $CH_3NH_3PbI_3$ or $CH(NH_2)_2PbI_3$. In our calculations, we have limited ourselves to perovskite film thicknesses in which the carrier collection probability (internal quantum efficiency) is close to unity. In the case of the $CH_3NH_3PbI_3$ – perovskite, the efficacy of our light-trapping architecture was shown by its ability to absorb sunlight beyond the Lambertian limit in the wavelength range of 300 nm – 800 nm. For this material, our photonic crystal design enabled a MAPD of 25.1 mA/cm^2 and a projected power-conversion efficiency of 12.9%. This corresponds to absorption of 92% of all available sunlight in the relevant wavelength range. Excellent solar absorption was retained over a broad incident angular range from 0 to 60 degrees. A

similar light-trapping enhancement of solar absorption in the wavelength range of 300 nm – 850 nm was found in the case of the $CH(NH_2)_2PbI_3$ – perovskite. For this material, our inverted cone photonic crystal design yields a MAPD of 29.1 mA/cm^2 using a film height of 450 nm. Several competing photonic crystal architectures appear near this film height. Interestingly, no further improvement in overall solar absorption was found by increasing the film thickness beyond 450 nm. By comparison of our calculated results with published experimental results on planar perovskite solar cells, we estimate a power-conversion efficiency of 23.4% in a corresponding, real-world, photonic crystal solar cell based on $CH(NH_2)_2PbI_3$. For both perovskites, we estimate a 15-17% improvement in power conversion efficiency relative to those of the best planar solar cell geometries. It is of interest to explore nano-imprinting methods for the fabrication of thin-film, inverted-cone photonic crystals. It is also of interest to study the possibility of deposition of perovskites onto thin-film Silicon photonic crystals[31] to realized very high-efficiency tandem solar cells.

ACKNOWLEDGEMENT

[1] A. Kojima, K. Teshima, Y. Shirai, and T. Miyasaka, "Organometal Halide Perovskites as Visible-Light Sensitizers for Photovoltaic Cells," J. Am. Chem. Soc. **131**, 6050–6051 (2009).

[2] M. M. Lee, J. Teuscher, T. Miyasaka, T. N. Murakami, and H. J. Snaith, "Efficient Hybrid Solar Cells Based on Meso-Superstructured Organometal Halide Perovskites," Sci **338**, 643–647 (2012).

[3] H.-S. Kim, J.-W. Lee, N. Yantara, P. P. Boix, S. A. Kulkarni, S. Mhaisalkar, M. Grätzel, and N.-G. Park, "High Efficiency Solid-State Sensitized Solar Cell-Based on Submicrometer Rutile TiO2 Nanorod and CH3NH3PbI3 Perovskite Sensitizer," Nano Lett. **13**, 2412–2417 (2013).

[4] X. Gao, J. Li, J. Baker, Y. Hou, D. Guan, J. Chen, and C. Yuan, "Enhanced photovoltaic performance of perovskite CH3NH3PbI3 solar cells with freestanding TiO2 nanotube array films," Chem. Commun. **50**, 6368–6371 (2014).

[5] Q. Jiang, X. Sheng, Y. Li, X. Feng, and T. Xu, "Rutile TiO2 nanowire-based perovskite solar cells," Chem. Commun. **50**, 14720–14723 (2014).

[6] J.-H. Im, J. Luo, M. Franckevičius, N. Pellet, P. Gao, T. Moehl, S. M. Zakeeruddin, M. K. Nazeeruddin, M. Grätzel, and N.-G. Park, "Nanowire Perovskite Solar Cell," Nano Lett. **15**, 2120–2126 (2015).

[7] S. S. Mali, C. S. Shim, H. K. Park, J. Heo, P. S. Patil, and C. K. Hong, "Ultrathin Atomic Layer Deposited TiO2 for Surface Passivation of Hydrothermally Grown 1D TiO2 Nanorod Arrays for Efficient Solid-State Perovskite Solar Cells," Chem. Mater. **27**, 1541–1551 (2015).

[8] X. Wang, Z. Li, W. Xu, S. A. Kulkarni, S. K. Batabyal, S. Zhang, A. Cao, and L. H. Wong, "TiO2 nanotube arrays based flexible perovskite solar cells with transparent carbon nanotube electrode," Nano Energy **11**, 728–735 (2015).

[9] M. Liu, M. B. Johnston, and H. J. Snaith, "Efficient planar heterojunction perovskite solar cells by vapour deposition," Nature **501**, 395–398 (2013).

[10] O. Malinkiewicz, A. Yella, Y. H. Lee, G. M. Espallargas, M. Graetzel, M. K. Nazeeruddin, and H. J. Bolink, "Perovskite solar cells employing organic charge-transport layers," Nat Photon **8**, 128–132 (2014).

[11] Q. Lin, A. Armin, R. C. R. Nagiri, P. L. Burn, and P. Meredith, "Electro-optics of perovskite solar cells," Nat Photon **9**, 106–112 (2015).

[12] N. J. Jeon, J. H. Noh, W. S. Yang, Y. C. Kim, S. Ryu, J. Seo, and S. I. Seok, "Compositional engineering of perovskite materials for high-performance solar cells," Nature **517**, 476–480 (2015).

[13] W. S. Yang, J. H. Noh, N. J. Jeon, Y. C. Kim, S. Ryu, J. Seo, and S. I. Seok, "High-performance photovoltaic perovskite layers fabricated through intramolecular exchange," Sci **348**, 1234–1237 (2015).

[14] J. M. Ball, S. D. Stranks, M. T. Horantner, S. Huttner, W. Zhang, E. J. W. Crossland, I. Ramirez, M. Riede, M. B. Johnston, R. H. Friend, and H. J. Snaith, "Optical properties and limiting photocurrent of thin-film perovskite solar cells," Energy & Environmental Science **8**, 602–609 (2015).

[15] B. W. Schneider, N. N. Lal, S. Baker-Finch, and T. P. White, "Pyramidal surface textures for light trapping and antireflection in perovskite-on-silicon tandem solar cells," Opt. Express **22**, A1422–A1430 (2014).

[16] M. Filipič, P. Löper, B. Niesen, S. De Wolf, J. Krč, C. Ballif, and M. Topič, "CH3NH3PbI3 perovskite / silicon tandem solar cells: characterization based optical simulations," Opt. Express **23**, A263–A278 (2015).

[17] L. Hu and G. Chen, "Analysis of Optical Absorption in Silicon Nanowire Arrays for Photovoltaic Applications," Nano Lett. **7**, 3249–3252 (2007).

[18] Q. G. Du, C. H. Kam, H. V. Demir, H. Y. Yu, and X. W. Sun, "Enhanced optical absorption in nanopatterned silicon thin films with a nano-cone-hole structure for photovoltaic applications," Opt. Lett. **36**, 1713–1715 (2011).

[19] S. Eyderman, S. John, and A. Deinega, "Solar light trapping in slanted conical-pore photonic crystals: Beyond statistical ray trapping," J. Appl. Phys. **113**, 154315 (2013).

[20] S. Eyderman, A. Deinega, and S. John, "Near perfect solar absorption in ultra-thin-film GaAs photonic crystals," Journal of Materials Chemistry A **2**, 761–769 (2014).

[21] D. H. Wang, J. Seifter, J. H. Park, D.-G. Choi, and A. J. Heeger, "Efficiency Increase in Flexible Bulk Heterojunction Solar Cells with a Nano-Patterned Indium Zinc Oxide Anode," Advanced Energy Materials **2**, 1319–1322 (2012).

[22] S. Foster and S. John, "Light trapping design for low band-gap polymer solar cells," Opt. Express **22**, A465–A480 (2014).

[23] *Electromagnetic Template Library (EMTL), Kintech Lab Ltd*, http://fdtd.kintechlab.com.

[24] M. Baum, I. Alexeev, M. Latzel, S. H. Christiansen, and M. Schmidt, "Determination of the effective refractive index of nanoparticulate ITO layers," Opt. Express **21**, 22754–22761 (2013).

[25] Air Mass 1.5 Spectra, American Society for Testing and Materials," retrieved: http://rredc.nrel.gov/solar/spectra/am1.5/.

[26] P. Löper, M. Stuckelberger, B. Niesen, J. Werner, M. Filipič, S.-J. Moon, J.-H. Yum, M. Topič, S. De Wolf, and C. Ballif, "Complex Refractive Index Spectra of CH3NH3PbI3 Perovskite Thin Films Determined by Spectroscopic Ellipsometry and Spectrophotometry," The Journal of Physical Chemistry Letters **6**, 66–71 (2015).

[27] S. D. Stranks, G. E. Eperon, G. Grancini, C. Menelaou, M. J. P. Alcocer, T. Leijtens, L. M. Herz, A. Petrozza, and H. J. Snaith, "Electron-Hole Diffusion Lengths Exceeding 1 Micrometer in an Organometal Trihalide Perovskite Absorber," Sci **342**, 341–344 (2013).

[28] E. Yablonovitch, "Statistical ray optics," J. Opt. Soc. Am. **72**, 899–907 (1982).

[29] J.-W. Lee, D.-J. Seol, A.-N. Cho, and N.-G. Park, "High-Efficiency Perovskite Solar Cells Based on the Black Polymorph of HC(NH2)2PbI3," Adv. Mater. **26**, 4991–4998 (2014).

[30] N. Pellet, P. Gao, G. Yang, M. K. Nazeeruddin, J. Maier, and M. Grätzel, "Mixed-Organic-Cation Perovskite Photovoltaics for Enhanced Solar-Light Harvesting," Angew. Chem. Int. Ed. **53**, 3151–3157 (2014).

[31] S. Eyderman, S. John, M. Hafez, S. S. Al-Ameer, T. S. Al-Harby, Y. Al-Hadeethi, and D. M. Bouwes, "Light-trapping optimization in wet-etched silicon photonic crystal solar cells," J. Appl. Phys. **118**, 023103 (2015).